PHYSICAL REVIEW D **80,** 074033 (2009)

Sivers asymmetries for inclusive pion and kaon production in deep-inelastic scattering

John Ellis,[1] Dae Sung Hwang,[2] and Aram Kotzinian[3,4,5]
[1]*Theory Division, Physics Department, CERN, 1211 Geneva 23, Switzerland*
[2]*Department of Physics, Sejong University, Seoul 143-747, South Korea*
[3]*CEA DAPNIA/SPhN Saclay, 91191 Gif-sur-Yvette, France*
[4]*Joint Institute for Nuclear Research, 141980 Dubna, Moscow region, Russia*
[5]*Yerevan Physics Institute, 375036 Yerevan, Armenia*
(Received 18 August 2008; published 27 October 2009)

We calculate the Sivers distribution functions induced by the final-state interaction due to one-gluon exchange in diquark models of a nucleon structure, treating the cases of scalar and axial-vector diquarks with both dipole and Gaussian form factors. We use these distribution functions to calculate the Sivers single-spin asymmetries for inclusive pion and kaon production in deep-inelastic scattering. We compare our calculations with the results of HERMES and COMPASS, finding good agreement for π^+ production at HERMES, and qualitative agreement for π^0 and K^+ production. Our predictions for pion and kaon production at COMPASS could be probed with increased statistics. The successful comparison of our calculations with the HERMES data constitutes *prima facie* evidence that the quarks in the nucleon have some orbital angular momentum in the infinite-momentum frame.

DOI: 10.1103/PhysRevD.80.074033 PACS numbers: 13.88.+e, 12.39.−x, 13.60.−r

I. INTRODUCTION

It is well known that transverse-momentum-dependent distribution and fragmentation functions can have a nontrivial spin dependences and that the so-called ''T-odd'' transverse-momentum-dependent distribution and fragmentation functions can lead to single-spin asymmetries [1–4]. They are also often referred to as ''naively T-odd,'' because the appearance of these functions does not imply a violation of time-reversal invariance, since they can arise through final-state interactions. The Sivers distribution function $f_{1T}^{\perp}$, schematically depicted in Fig. 1, is the oldest example of such a function.

It describes the difference between the momentum distributions of quarks inside protons transversely polarized in opposite directions. The Sivers effect was put forward as a possible explanation for the large single-spin asymmetries observed in $p^{\uparrow}p \to \pi X$ experiments [1,3,5]. Furthermore, it generates single-spin asymmetries in inclusive hadron production in deep-inelastic scattering (SIDIS) [4,6]. These have been measured by the HERMES collaboration to be nonzero for $lp^{\uparrow} \to l'\pi X$ [7], and updated HERMES results for pion and kaon production have been reported in [8]. More recently, COMPASS has analyzed their SIDIS data on pion and kaon production off a deuteron target [9], and collected data using a proton target in 2007. Phenomenological analyses of SIDIS data have been performed in Refs. [10–13]. The Sivers effect may also result, e.g., in asymmetric di-jet correlations in $p^{\uparrow}p \to$ jet jet X [14,15], but these are not yet visible in the data analyzed to date [16].

In recent years the importance in hadron physics of the role of the transverse momenta of the partons has been better recognized, since they provide time-odd distribution and fragmentation functions, and make possible single-spin asymmetries in hadronic processes [4,6,17]. Specifically, it has been understood that one-gluon-exchange final-state interactions (FSI) are a calculable mechanism for generating a transverse single-spin asymmetry in SIDIS [6]. This FSI generates a Sivers effect when the distribution functions are allowed to be functions of the transverse momenta of the partons, as well as their longitudinal momentum fractions. Therefore, taking the transverse momenta of the partons into consideration enlarges the realm of investigation of the nucleon structure.

A simple scalar diquark model was used in [6] to demonstrate explicitly that this FSI can indeed give rise to a leading-twist transverse single-spin asymmetries in SIDIS, which emerged from interference between spin-dependent amplitudes for different nucleon spin states. It was observed in [6,18] that the same overlap integrals between light-cone wave functions that describe the contribution to the nucleon anomalous magnetic moment from a given quark flavor also appear in the Sivers distribution for that quark flavor (with additional pieces in the integrand). Since these integrals are the overlaps between light-cone wave functions whose orbital angular momenta differ by $\Delta L^z = \pm 1$, nonzero orbital angular momenta of the quarks inside the proton are essential for the existence of the Sivers asymmetry [6,18].

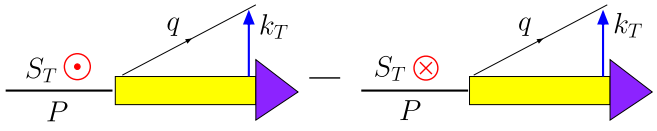

FIG. 1 (color online). Schematic depiction of the Sivers distribution function $f_{1T}^{\perp}$. The spin vector S_T of the nucleon points out of and into the page, respectively, and k_T is the transverse momentum of the extracted quark.

A more realistic model for time-even transverse-momentum-dependent parton distributions was considered in [19], namely, a quark-diquark model with both scalar and axial-vector diquarks, as suggested by the simple SU(6) quark model of the nucleon. The FSI approach was recently applied within this type of model also for time-odd quark distributions in [20–22]. The authors of [21] considered different choices of the diquark propagator and gluon-diquark vertex. A more general nucleon–quark-diquark vertex and a general form of gluon-diquark vertex have also been considered in [22]. We note that the simple quark-diquark model is only a naive description of the nucleon, and is applicable only for valence quarks. In this paper we present results obtained within this model with the simplest choices for the nucleon–quark-diquark vertex, the gluon-diquark vertex, and the diquark propagator.

We calculate the Sivers distribution functions in SIDIS induced by the one-gluon exchange final-state interaction for models of the nucleon in which the spectator diquark is treated as either a scalar or an axial-vector. As we discuss below, the simplest SU(6) wave function of the nucleon suggests that the spectator diquark would be in a combination of these two states. We consider two types of form factor at the nucleon–quark-diquark vertices: the dipole form factor used by Jakob *et al.* in [19] and the Gaussian form factor used by Gamberg *et al.* in [23,24]. When either of these form factors is used, we find that at larger transverse momenta the asymmetry calculated using a one-gluon exchange may exceed unity in magnitude, indicating that unknown higher-order effects must become important there.[1] Imposing the physical restriction that the asymmetry calculated by one-gluon exchange not exceed unity changes rather little the Sivers single-spin asymmetry after integration over the transverse momentum, indicating that the results we present should be quite reliable. The similarity of our predictions for dipole and Gaussian form factors also indicates the stability of our results.

We compare our results for the Sivers single-spin asymmetries for π^+, π^0, π^-, K^+, and K^- with the SIDIS measurements made by HERMES and COMPASS. We find good agreement with the HERMES results for π^+ production, and qualitative agreement for π^0 and K^+ production. The experimental errors in the HERMES measurements of the Sivers asymmetries for π^- and K^- production do not permit any definite conclusions to be drawn. The same is true of the current measurements by COMPASS, and we look forward to increased statistics that could further test our predictions for pion and kaon production in SIDIS. However, the successful comparison of our calculations with the HERMES data already constitutes *prima facie* evidence that the longitudinal projection of the net quark angular momentum in the infinite-momentum frame is nonzero.

[1]A more complete description of the FSI can be made by introducing an appropriate Wilson-line phase factor in the definition of the distribution functions of quarks in the nucleon [1,25–28].

II. BASIC FORMULAS FOR THE SIVERS ASYMMETRY

A. Definition of the Sivers asymmetry $A_{\rm UT}^{\sin(\phi_h-\phi_S)}(x)$

The SIDIS cross section $l + N^\uparrow \to l' + h + X$ on a transversely-polarized (T) target contains 8 spin-dependent azimuthal modulations. Here we consider only one of them—the so-called Sivers asymmetry. The relevant angular distribution of the cross section contains unpolarized (U) and Sivers (Siv) parts:

$$\frac{d^6\sigma(x,y,z,P_T,\phi_h,\phi_S)}{dxdydzd^2P_Td\phi_S} = \frac{d^6\sigma_{\rm U}(x,y,z,P_T,\phi_h)}{dxdydzd^2P_Td\phi_S} + S_T\frac{d^6\sigma_{\rm Siv}(x,y,z,P_T)}{dxdydzd^2P_Td\phi_S}\times\sin(\phi_h-\phi_S), \tag{1}$$

where ϕ_h and ϕ_S are the azimuthal angles of the transverse momentum of the produced hadron and the transverse spin of the target relative to the virtual photon direction.

The Sivers asymmetry is usually defined as

$$A_{\rm UT}^{\sin(\phi_h-\phi_S)}(x,y,z,P_T) = \frac{2}{S_T}\frac{\int d\phi_h\int d\phi_S d^6\sigma(x,y,z,P_T,\phi_h,\phi_S)\sin(\phi_h-\phi_S)}{\int d\phi_h\int d\phi_S d^6\sigma(x,y,z,P_T,\phi_h,\phi_S)}, \tag{2}$$

and we note that the integration singles out the $\sigma_{\rm U}$ component in the denominator and $\sigma_{\rm Siv}$ in the numerator.

Within the LO QCD parton model, we have

$$\frac{d^6\sigma_{\rm U}(x,y,z,P_T,\phi_h)}{dxdydzd^2P_Td\phi_S} = C(x,y)\Sigma_q e_q^2\int d^2\mathbf{k}_\perp^2 f_1^q(x,\mathbf{k}_\perp^2)D_{1q}^h(z,\mathbf{p}_\perp^2), \tag{3}$$

$$\frac{d^6\sigma_{\rm Siv}(x,y,z,P_T)}{dxdydzd^2P_Td\phi_S} = C(x,y)\Sigma_q e_q^2\int d^2\mathbf{k}_\perp\left(-\frac{|\mathbf{k}_\perp|}{M}\right)\times\sin(\phi_q-\phi_S)f_{1T}^{\perp q}(x,\mathbf{k}_\perp^2)D_{1q}^h(z,\mathbf{p}_\perp^2), \tag{4}$$

where

$$C(x,y) = \frac{\alpha_{em}^2}{2ME}\frac{1+(1-y)^2}{xy^2}, \tag{5}$$

$f_1^q(x,\mathbf{k}_\perp)$ and $f_{1T}^{\perp q}(x,\mathbf{k}_\perp)$ are the unpolarized and Sivers quark distribution functions inside the nucleon, ϕ_q is the azimuthal angle of the active quark q, $D_{1q}^h(z,\mathbf{p}_\perp)$ is the unpolarized fragmentation function of q into the hadron h, and

$$\mathbf{p}_\perp = \mathbf{P}_T - z\mathbf{k}_\perp \tag{6}$$

is the transverse momentum of the produced hadron with respect to the fragmenting quark momentum.

In order to obtain the dependence of Sivers asymmetry on any single kinematic variable such as x, one must integrate the unpolarized and polarization-dependent parts of the cross sections over the other three kinematic variables:

$$A_{\mathrm{UT}}^{\sin(\phi_h-\phi_S)}(x) = \frac{\Delta\hat{\sigma}(x)}{\hat{\sigma}(x)}, \tag{7}$$

$$\Delta\hat{\sigma}(x) = \mathrm{Int}\Big[C(x,y)\Sigma_q e_q^2 \int d^2\mathbf{k}_\perp \Big(-\frac{\mathbf{k}_\perp\cdot\mathbf{P}_T}{M|\mathbf{P}_T|}\Big) \times f_{1T}^{\perp q}(x,\mathbf{k}_\perp) D_{1q}^h(z,\mathbf{P}_T - z\mathbf{k}_\perp)\Big], \tag{8}$$

$$\hat{\sigma}(x) = \mathrm{Int}\Big[C(x,y)\Sigma_q e_q^2 \int d^2\mathbf{k}_\perp f_1^q(x,\mathbf{k}_\perp) \times D_{1q}^h(z,\mathbf{P}_T - z\mathbf{k}_\perp)\Big], \tag{9}$$

where Int[...] denotes the following integration:

$$\mathrm{Int}[G] = \int_{z_{\min}}^{z_{\max}} dz \int_{P_{T\min}}^{P_{T\max}} d|\mathbf{P}_T||\mathbf{P}_T| \int_0^{2\pi} d\phi \times \int_0^{k_{\perp\max}} d|\mathbf{k}_\perp||\mathbf{k}_\perp|[G]. \tag{10}$$

The derivation of (8) is given in the Sec. II B.

In the later comparisons with experimental data, we use the following integration limits for asymmetries on a proton target at HERMES: $0.2 < z < 0.8$, 0.05 GeV $< |\mathbf{P}_T| <$ 1.2 GeV, and for asymmetries on a deuteron target at COMPASS we use $0.2 < z < 0.8$, 0.1 GeV $< |\mathbf{P}_T| <$ 2.0 GeV, corresponding to the kinematic conditions of these experiments.

B. Intrinsic $\mathbf{k}_\perp$ integration

Let us consider two integrals:

$$R_1 = \int d^2\mathbf{k}_\perp f(\mathbf{k}_\perp^2) D(\mathbf{p}_\perp^2), \tag{11}$$

$$R_2 = \int d^2\mathbf{k}_\perp \frac{|\mathbf{k}_\perp|}{M} \sin(\phi_q - \phi_S) f(\mathbf{k}_\perp^2) D(\mathbf{p}_\perp^2). \tag{12}$$

The integrand of R_1 is a scalar function of vectors $\mathbf{k}_\perp$ and $\mathbf{P}_T$ in the two-dimensional transverse-momentum space. This means that R_1 can be a function only of z and $\mathbf{P}_T^2$:

$$R_1 = r_1(z,\mathbf{P}_T^2).$$

On the other hand, (12) can be represented as

$$R_2 = \hat{S}_1 F_2 - \hat{S}_2 F_1, \tag{13}$$

where $\hat{S}_{1,2}$ are the components of the two-dimensional transverse spin vector $\hat{\mathbf{S}}$ and the F_i are the components of

$$\mathbf{F} = \int d^2\mathbf{k}_\perp \frac{\mathbf{k}_\perp}{M} f(\mathbf{k}_\perp^2) D(\mathbf{p}_\perp^2). \tag{14}$$

Since $\mathbf{F}$ is a two-dimensional vector, and the only vector remaining after integration in (14) is $\mathbf{P}_T$, we have

$$\mathbf{F} = \mathbf{P}_T \Phi(\mathbf{P}_T^2), \tag{15}$$

and hence

$$\Phi(\mathbf{P}_T^2) = \frac{\mathbf{P}_T\cdot\mathbf{F}}{\mathbf{P}_T^2}. \tag{16}$$

From Eqs. (13)–(16) we finally obtain

$$R_2 = \sin(\phi_h - \phi_S) r_2(z,\mathbf{P}_T^2),$$

where

$$r_2(z,\mathbf{P}_T^2) = \int d^2\mathbf{k}_\perp \frac{\mathbf{k}_\perp\cdot\mathbf{P}_T}{M|\mathbf{P}_T|} f(\mathbf{k}_\perp^2) D(\mathbf{p}_\perp^2). \tag{17}$$

C. Calculations of the Sivers function in diquark models

In this subsection we repeat the derivation of the Sivers function in the scalar diquark model with a constant Yukawa vertex given in [6,29], and later generalize the result to the scalar and axial-vector diquark models with nontrivial form factors $g(k^2)$ at the nucleon–quark-diquark vertex. We obtain, from (A6) in the Appendix of this paper or from (22) of [29], the following expression for the distribution function in the Yukawa model:

$$f_1(x,\mathbf{k}_\perp) = g^2(1-x)\frac{\mathbf{k}_\perp^2 + (xM+m)^2}{(\mathbf{k}_\perp^2 + B)^2}. \tag{18}$$

From Eqs. (28) and (30) of [29], we also have

$$k_\perp^x f_{1T}^\perp(x,\mathbf{k}_\perp) = -g^2\frac{e_1e_2}{4\pi}(xM+m)(1-x)\frac{1}{(\mathbf{k}_\perp^2+B)}\frac{1}{\pi} \times \int d^2\boldsymbol{l}_\perp \frac{1}{(\boldsymbol{l}_\perp^2+B)}\frac{(l_\perp - k_\perp)^x}{[(\boldsymbol{l}_\perp - \mathbf{k}_\perp)^2 + \lambda_g^2]}. \tag{19}$$

Here we set to unity the parameter a in Eq. (30) of [29]. Using (18) and (19), we can write

$$\frac{f_{1T}^\perp(x,\mathbf{k}_\perp)}{f_1(x,\mathbf{k}_\perp)} = \frac{e_1e_2}{4\pi}\frac{M(xM+m)}{(xM+m)^2+\mathbf{k}_\perp^2} k_\perp^x R(x,\mathbf{k}_\perp), \tag{20}$$

where $R(x,\mathbf{k}_\perp)$ is given by

$$k_\perp^x R(x,\mathbf{k}_\perp)\times\frac{1}{\mathbf{k}_\perp^2+B}=\frac{-1}{\pi}\int d^2\boldsymbol{l}_\perp\frac{1}{(\boldsymbol{l}_\perp^2+B)}\times\frac{(l_\perp-k_\perp)^x}{[(\boldsymbol{l}_\perp-\mathbf{k}_\perp)^2+\lambda_g^2]}\equiv I. \tag{21}$$

We calculate the right-hand side of (21) by first taking the direction of $\mathbf{k}_\perp$ as the x direction and using k and l to denote $|\mathbf{k}_\perp|$ and $|\boldsymbol{l}_\perp|$, respectively, so that

$$\begin{aligned}\mathbf{k}_\perp&=k(1,0),\\ \boldsymbol{l}_\perp&=l(\cos\phi,\sin\phi),\\ (l_\perp-k_\perp)^x&=l\cos\phi-k,\\ (\boldsymbol{l}_\perp-\mathbf{k}_\perp)&=(l\cos\phi-k,l\sin\phi),\\ (\boldsymbol{l}_\perp-\mathbf{k}_\perp)^2&=l^2+k^2-2kl\cos\phi.\end{aligned} \tag{22}$$

Then, I in (21) becomes

$$I=\frac{-1}{\pi}\int ldld\phi\frac{l\cos\phi-k}{(l^2+B)(l^2+k^2-2kl\cos\phi)}=\int_0^\infty ldl\frac{1}{(l^2+B)(l^2+k^2)}\left(\frac{-1}{\pi}\int_0^{2\pi}d\phi\frac{l\cos\phi-k}{1-\frac{2kl}{l^2+k^2}\cos\phi}\right). \tag{23}$$

After some calculations, we find that the last factor in (23) gives

$$\left(\frac{-1}{\pi}\int_0^{2\pi}d\phi\frac{l\cos\phi-k}{1-\frac{2kl}{l^2+k^2}\cos\phi}\right)=\begin{cases}2\frac{l^2+k^2}{k} & \text{when } l<k\\ 0 & \text{when } l>k\end{cases}. \tag{24}$$

Using (24), the expression (23) becomes

$$I=\int_0^k ldl\frac{1}{(l^2+B)(l^2+k^2)}2\frac{l^2+k^2}{k}=\frac{1}{k}\int_0^k 2ldl\frac{1}{(l^2+B)}=\frac{k_\perp^x}{\mathbf{k}_\perp^2}\int_0^{\mathbf{k}_\perp^2}d(\boldsymbol{l}_\perp^2)\frac{1}{(\boldsymbol{l}_\perp^2+B)}, \tag{25}$$

where we use $1/k=k_\perp^x/\mathbf{k}_\perp^2$, since we take the direction of $\mathbf{k}_\perp$ as the x direction. From (21) and (25), we have

$$R(x,\mathbf{k}_\perp)\times\frac{1}{\mathbf{k}_\perp^2+B}=\frac{1}{\mathbf{k}_\perp^2}\int_0^{\mathbf{k}_\perp^2}d(\boldsymbol{l}_\perp^2)\frac{1}{(\boldsymbol{l}_\perp^2+B)}. \tag{26}$$

Then, using $R(x,\mathbf{k}_\perp)$ in (26), we can obtain the Sivers function from the formula (20). The result is identical to the result in [6,29].

Equation (26) is for the Yukawa model, presented in the Appendix, in which the nucleon–quark-diquark vertex is $g(k^2)=1$. We can generalize (26) for a general form factor $g(k^2)=g(x,\mathbf{k}_\perp)$ by using the following formula:

$$R(x,\mathbf{k}_\perp)\times\frac{g(x,\mathbf{k}_\perp)}{\mathbf{k}_\perp^2+B}=\frac{1}{\mathbf{k}_\perp^2}\int_0^{\mathbf{k}_\perp^2}d(\boldsymbol{l}_\perp^2)\frac{g(x,\boldsymbol{l}_\perp)}{(\boldsymbol{l}_\perp^2+B)}. \tag{27}$$

Using formula (27), we now calculate $R(x,\mathbf{k}_\perp)$ for the dipole and Gaussian form factors at the proton–quark-diquark vertex, respectively, obtaining the results shown in (39) and (49).

D. Generalized diquark models

While the simplest possibility for the spectator diquark is the scalar case, even in the absence of orbital angular momentum in the nucleon rest frame, it may exist in a spin-one, axial-vector state. Indeed, this possibility is realized in the simplest nonrelativistic SU(6) wave function for the proton:

$$\begin{aligned}|p\uparrow\rangle=&\frac{1}{\sqrt{3}}\left(\sqrt{\frac{2}{3}}|uu1+1\rangle|d\downarrow\rangle-\sqrt{\frac{1}{3}}|uu10\rangle|d\uparrow\rangle\right)\\&-\frac{1}{\sqrt{6}}\left(\sqrt{\frac{2}{3}}|ud1+1\rangle|u\downarrow\rangle-\sqrt{\frac{1}{3}}|ud10|u\uparrow\rangle\right)\\&+\frac{1}{\sqrt{2}}|ud00>|u\uparrow\rangle\end{aligned} \tag{28}$$

$$\begin{aligned}|p\downarrow\rangle=&\frac{1}{\sqrt{3}}\left(-\sqrt{\frac{2}{3}}|uu1-1\rangle|d\uparrow\rangle+\sqrt{\frac{1}{3}}|uu10\rangle|d\downarrow\rangle\right)\\&-\frac{1}{\sqrt{6}}\left(-\sqrt{\frac{2}{3}}|ud1-1>|u\uparrow\rangle+\sqrt{\frac{1}{3}}|ud10\rangle|u\downarrow\rangle\right)\\&+\frac{1}{\sqrt{2}}|ud00\rangle|u\downarrow\rangle.\end{aligned} \tag{29}$$

In each of the terms in (28) and (29), we have exhibited the spin states of the spectator diquark, showing explicitly that it is in a combination of scalar and axial-vector configurations in different spin states.

If the proton does have a naive SU(6) wave function in its rest frame, the distribution functions of the u and d quarks inside the proton, f_1^u and f_1^d, are given by

$$f_1^u=\tfrac{3}{2}f_1^s+\tfrac{1}{2}f_1^a,\qquad f_1^d=f_1^a, \tag{30}$$

and those inside the deuteron are given by

$$f_{\text{deu }1}^u=f_{\text{deu }1}^d=f_1^u+f_1^d. \tag{31}$$

The same relations also hold for the Sivers distribution functions, as we discuss below in more detail.

In the following, we allow for nontrivial form factors at the nucleon–quark-diquark vertices, in both the scalar (s) and axial-vector (a) diquark cases:

$$\Upsilon_s=g_s(k^2),\qquad \Upsilon_a^\mu=\frac{g_a(k^2)}{\sqrt{3}}\gamma^\mu\gamma_5. \tag{32}$$

Two specific models for the form factors $g_s(k^2)$ and $g_a(k^2)$ are discussed in the following sections.

Using the diquark model for the nucleon with specific forms for the vertices and polarization vectors, Ref. [19] obtained reasonably good T-even distribution functions for

the nucleon. Ref. [19] used the nucleon-quark-diquark vertex given by $\Upsilon^\mu_a = \frac{g_a(k^2)}{\sqrt{3}}\gamma_5(\gamma^\mu + \frac{P^\mu}{M})$. Since Ref. [19] used the polarization vectors which satisfy $\sum_\lambda \epsilon^{(\lambda)*}_\mu \epsilon^{(\lambda)}_\nu = -g_{\mu\nu} + P_\mu P_\nu/M^2$, the second term $\frac{g_a(k^2)}{\sqrt{3}}\gamma_5\frac{P^\mu}{M}$ in their Υ^μ_a vanishes when it is multiplied by the polarization vectors. Therefore, the vertex Υ^μ_a in (32) of our paper is equivalent to that used in Ref. [19] with an overall minus sign difference. Hence, in this paper we use vertices and polarization vectors that are equivalent to those of Ref. [19], i.e., essentially we work with the diquark model for the nucleon presented in Ref. [19]. We find in the Appendix that this model gives axial-vector diquark wave functions that, in the nucleon rest frame, coincide with the wave functions of the spin-half states that are made by adding spin-half and spin-one states with the correct Clebsch-Gordan coefficients. Therefore, this model is consistent with the SU(6) wave function of the nucleon. We note that Ref. [30] considered general vertices that transform as a scalar or vector under Lorentz transformations.

III. DIPOLE FORM FACTOR

A. Calculations

We first consider a dipole model for the nucleon–quark-diquark vertex:

$$g_R(k^2) = \sqrt{N_R}\frac{k^2 - m^2}{(k^2 - \Lambda^2)^2} = \sqrt{N_R}\frac{(k^2 - m^2)(1-x)^2}{(\mathbf{k}_\perp^2 + B_R)^2}, \tag{33}$$

where $R = s$ for the scalar and $R = a$ for the axial-vector diquark, we used [19,29]

$$-k^2(x, \mathbf{k}_\perp^2) = \frac{\mathbf{k}_\perp^2}{1-x} + \frac{x}{1-x}M_R^2 - xM^2, \tag{34}$$

and B_R is given by

$$B_R = (1-x)\Lambda^2 + xM_R^2 - x(1-x)M^2. \tag{35}$$

We then have the following distribution functions from Fig. 2:

$$f_1^R(x, \mathbf{k}_\perp) = \frac{N_R}{16\pi^3}\frac{(1-x)^3[(xM+m)^2 + \mathbf{k}_\perp^2]}{(\mathbf{k}_\perp^2 + B_R)^4}, \tag{36}$$

yielding the following when integrated over $\mathbf{k}_\perp$:

$$f_1^R(x) = \frac{N_R}{16\pi^3}\frac{\pi(1-x)^3[2(xM+m)^2 + B_R]}{6B_R^3}. \tag{37}$$

The normalization factors N_R are fixed from the condition

$$\int_0^1 dx f_1^R(x) = 1. \tag{38}$$

In the present cases of dipole form factors, we obtain from (27)

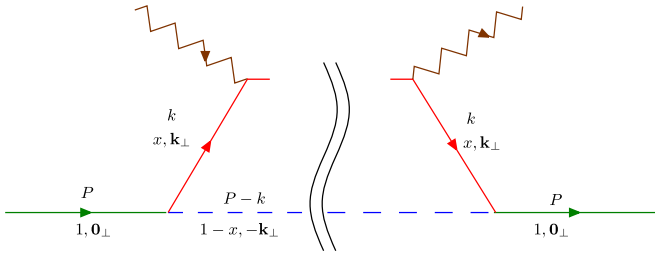

FIG. 2 (color online). Leading-order diagram contributing to f_1 in a diquark model.

$$R(x, \mathbf{k}_\perp)\times\frac{1}{(\mathbf{k}_\perp^2 + B_\Lambda)^2} = \frac{1}{\mathbf{k}_\perp^2}\int_0^{\mathbf{k}_\perp^2} d(l_\perp^2)\frac{1}{(l_\perp^2 + B_\Lambda)^2}$$
$$= \frac{1}{\mathbf{k}_\perp^2}\left(-\frac{1}{\mathbf{k}_\perp^2 + B_\Lambda} + \frac{1}{B_\Lambda}\right)$$
$$= \frac{1}{B_\Lambda(\mathbf{k}_\perp^2 + B_\Lambda)}. \tag{39}$$

Thus, we obtain finally the Sivers distribution functions for the dipole form factors as follows:

$$f_{1T}^{\perp R}(x, \mathbf{k}_\perp) = a_R\frac{e_1e_2}{4\pi}\frac{N_R(1-x)^3M(xM+m)}{16\pi^3B_R(\mathbf{k}_\perp^2 + B_R)^3}, \tag{40}$$

Following [6], we fix $\frac{e_1e_2}{4\pi} = -C_F\alpha_S$, where $C_F = \frac{4}{3}$.

In deriving (40), we use for the gauge-field coupling to the axial-vector diquark in Fig. 3 the simple form $ie_2g^{\alpha\beta}((P-l) + (P-k))^\mu$, which is equivalent, for each polarization state, to the gauge-field coupling to a scalar diquark. We motivate this simple coupling by assuming that the QCD coupling to the diquark is independent of the spin state of the diquark.

We note that the results for the axial-vector diquark in (36), (37), and (40) are different from those of [20], which are obtained if $\sum_\lambda \epsilon^{(\lambda)*}_\mu \epsilon^{(\lambda)}_\nu = -g_{\mu\nu}$ is used. Ref. [21] considers various different possibilities for the polarization sum of the axial-vector diquark. More general forms of gauge-field coupling to the axial-vector diquark were used in Refs. [20–22]. Ref. [22] used a more general nucleon–quark-diquark vertex for the axial-vector diquark.

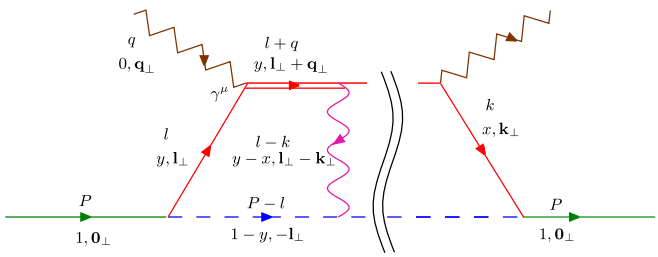

FIG. 3 (color online). Leading-order diagram contributing to the Sivers function $f_{1T}^\perp$ in a diquark model, via a one-gluon exchange FSI.

The values of a_R are given by the overlaps of the proton wave functions of positive and negative helicities. We find

$$a_s = 1 \quad \text{and} \quad a_a = -\tfrac{1}{3}. \tag{41}$$

Details of the derivation are presented in the Appendix, where the relations between the SU(6) and light-cone wave functions are discussed, as well as the relations between light-cone and Bjorken-Drell spinors.

In this paper we work with the diquark model for the nucleon presented in Ref. [19], as we explained in the last paragraph of Sec. II. In this model we obtained the wave functions (A16) and (A18) given in the Appendix for the quark and axial-vector diquark system. The Sivers distribution function $f_{1T}^{\perp}$ is given by the overlaps of the proton wave functions of positive and negative helicities [6,29]. As we can see in (A16) and (A18), only the wave functions with $s_b^z = 0$ contribute to the overlaps for $f_{1T}^{\perp}$. We find that the wave functions with $s_b^z = 0$ in (A16) and (A18) have the exactly same structures as the wave functions for the quark and scalar diquark system given in (A6) and (A10), except for the overall constant factor $-\frac{1}{\sqrt{3}}$ for the positive helicity wave functions and $+\frac{1}{\sqrt{3}}$ for the negative helicity ones. Therefore, the overlaps of positive and negative helicities for the quark and axial-vector diquark system have an overall factor of $-\frac{1}{3}$ compared to the overlaps of (A6) and (A10) for the quark and scalar diquark system. This is the reason why, in the diquark model with which we work in this paper, we have the same Sivers distribution functions for the cases of the scalar diquark and axial-vector diquark, except for the difference of the overall constant factors a_R given in (41).

We use $\alpha_S \approx 0.3$ and choose the following values for the parameters of the model studied in this section:

$$\begin{aligned} m &= 0.36 \text{ GeV}, \qquad M_s = 0.6 \text{ GeV}, \\ M_a &= 0.8 \text{ GeV}, \qquad \Lambda = 0.65 \text{ GeV}. \end{aligned} \tag{42}$$

We assume a Gaussian transverse-momentum dependence for the fragmentation functions:

$$D_{1q}^h(z, \mathbf{p}_\perp^2) = \frac{1}{\pi \mu_2^2} e^{-\mathbf{p}_\perp^2/\mu_2^2} D_{1q}^h(z), \tag{43}$$

with $\mu_2^2 = 0.2$ GeV^2 as obtained in [31]. We use the leading-order fragmentation functions of [32] for the integrated fragmentation functions $D_{1q}^h(z)$. The $\mathbf{k}_\perp$ integration is performed as described in Section II B.

We present in the top panel of Fig. 4 the dependence of the calculated asymmetry on the upper limit in the $\mathbf{k}_\perp$ integral. As one can see, the saturation of the integral takes place around 2 GeV, which is a rather high value, though about 90% of the integral is provided by the region $|\mathbf{k}_\perp| < 1$ GeV. For definiteness, in this section using dipole form factors, we use $|\mathbf{k}_\perp|_{\max} = 2.5$ GeV for the upper limit of the $\mathbf{k}_\perp$ integration. The leading-order perturbative QCD approach is believed to be applicable to SIDIS when all

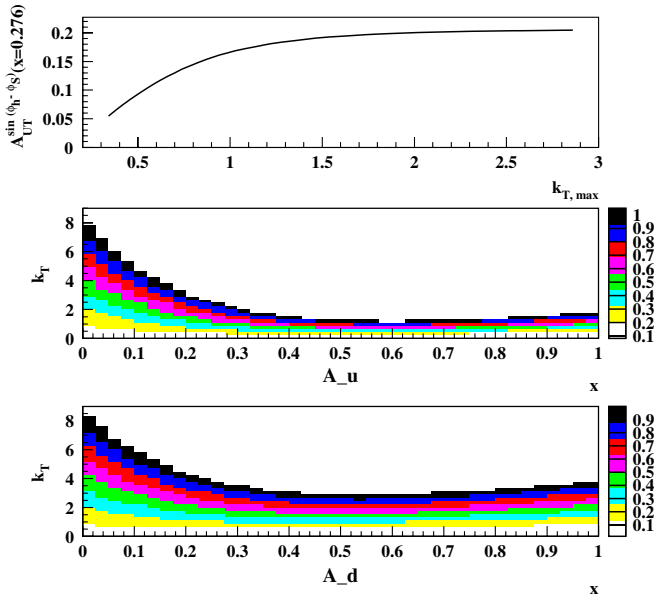

FIG. 4 (color online). In the top panel, we show the Sivers asymmetry for π^+ production off a proton target for HERMES kinematics at $x = 0.276$ as a function of the upper limit of the $|\mathbf{k}_\perp|$ integration. The analyzing power of the Sivers function for scattering off a u quark (middle panel) and a d quark (bottom panel) as functions of x and $k_T = |\mathbf{k}_\perp|$. The calculated values exceed the unitarity limit in the white regions at larger x and k_T. All these plots are obtained using dipole form factors.

transverse momenta are much smaller than the virtuality of the hard scattering, Q. However, in SIDIS at fixed energy there is a strong correlation between the mean values of x and Q^2: for example, at HERMES $\langle Q^2 \rangle (x = 0.18) \approx 4$ GeV^2 and $\langle Q^2 \rangle (x = 0.28) \approx 6$ GeV^2. Thus the highest virtuality at HERMES corresponding to the last populated x bins is of the same order of magnitude as the saturation value for the intrinsic transverse-momentum integration. This consideration, together with the fact that the simple diquark model used here treats only the valence quarks, shows that this approach cannot be considered reliable for low values of x. Hence, our results should be considered as applicable only to $x > 0.1$.

Another issue bearing on the accuracy of our results is that unitarity requires the analyzing power of the Sivers function to be less than unity in modulus for all values of x and $\mathbf{k}_\perp$: $A_{u,d} \equiv |k_\perp f_{1T}^{\perp u,d}(x, \mathbf{k}_\perp)/M f_1^{u,d}(x, \mathbf{k}_\perp)| \leq 1$. This is not always the case for the simplified leading-order one-gluon-exchange FSI that we consider, which tends to yield larger values at large x and $\mathbf{k}_\perp$, as seen in the middle panel of Fig. 4 for scattering off a u quark, and in the bottom panel for scattering off a d quark.[2] The issue would be resolved if a full higher-order calculation were performed,

[2]A related issue is that the asymmetry we calculate is large close to the contour in the $(x, \mathbf{k}_\perp)$ beyond which unitarity is violated.

but this is currently not available, so one must estimate the error incurred by including unphysical values in the integration over $\mathbf{k}_\perp$. In fact, we find that the naive predictions obtained by ignoring the unitarity issue differ from the modified calculations that are obtained by truncating the $\mathbf{k}_\perp$ integration at the x-dependent unitarity limit shown in Fig. 4, by far less than the present experimental uncertainties, so this theoretical error may be neglected for the time being.

B. Comparisons with data

In Figs. 5 and 6 we compare the Sivers asymmetries for pion and kaon production calculated with a dipole form factor using $\alpha_s = 0.3$ and $\Lambda = 0.65$ GeV with data from the HERMES Collaboration obtained using a proton target, and with data from the COMPASS Collaboration obtained using a deuteron target. In this paper we work with a simple diquark model in which only the valence u and d quarks of the nucleon are considered for the unpolarized and Sivers quark distribution functions inside the nucleon. Working within such an approximation, the different results for pion and kaon production in our calculation arise only from the difference of the fragmentation functions $D_{1q}^h(z)$ in Eq. (43) for pion and kaon productions from the u and d quarks, which are given in Ref. [32].

We see that our predictions for the π^+ asymmetry (top panel of Fig. 5) agree very well with the HERMES data, which exhibit a relatively significant positive asymmetry. The HERMES data for the π^- asymmetry (middle panel) are more equivocal, though they are compatible with positive values that are smaller than for π^+, as predicted by our calculations. We also predict a positive asymmetry for π^0 production, which is in qualitative agreement with the HERMES data, as seen in the bottom panel of Fig. 5. In

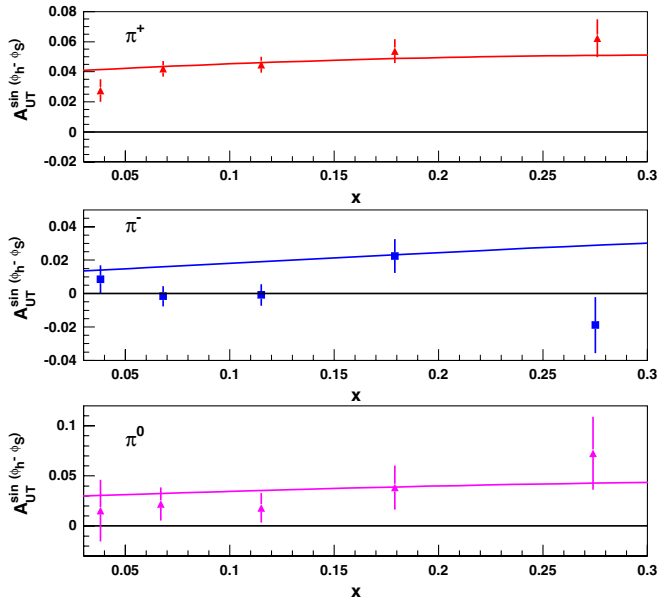

FIG. 5 (color online). Comparisons of our predictions for the Sivers asymmetries in the production of π^+ (top panel), π^- (middle panel), and π^0 (bottom panel) with HERMES data, assuming $\alpha_s = 0.3$ and $\Lambda = 0.65$ GeV for the dipole model parameters.

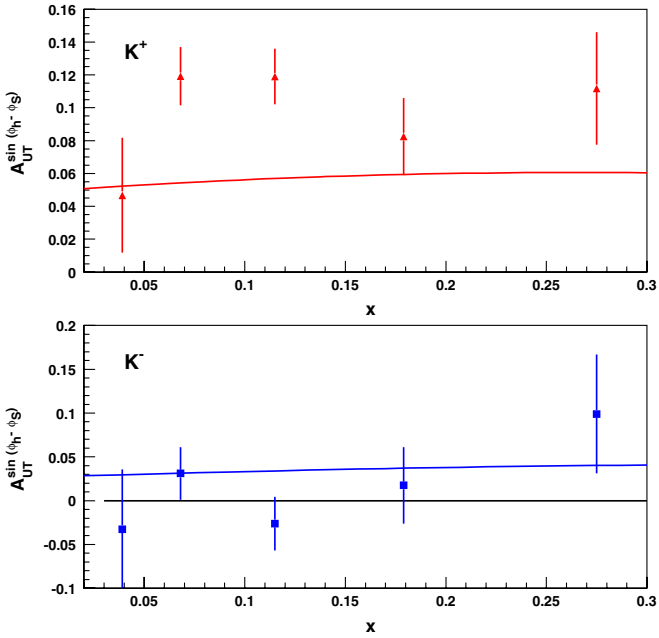

FIG. 6 (color online). Comparisons of our predictions for the Sivers asymmetries in the production of K^+ (top panel) and K^- (bottom panel) with HERMES data, assuming $\alpha_s = 0.3$ and $\Lambda = 0.65$ GeV for the dipole model parameters.

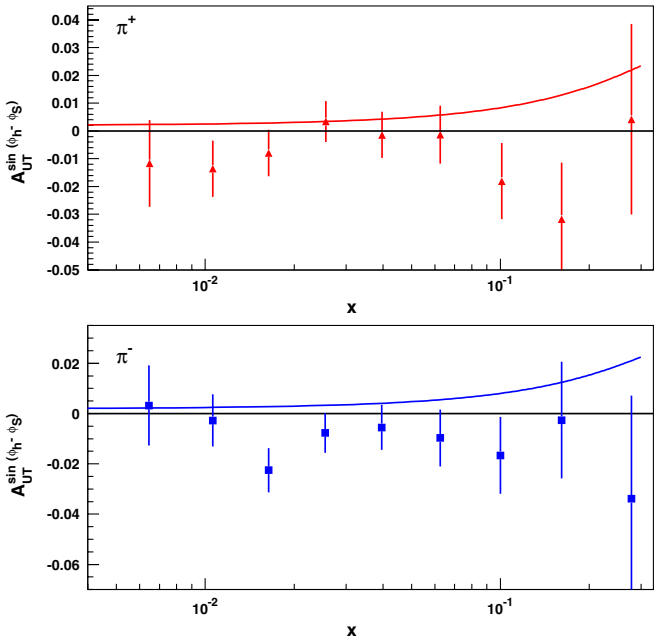

FIG. 7 (color online). Comparisons of our predictions for the Sivers asymmetries in the production of π^+ (top panel) and π^- (bottom panel) with COMPASS deuteron target data, assuming $\alpha_s = 0.3$ and $\Lambda = 0.65$ GeV for the dipole model parameters.

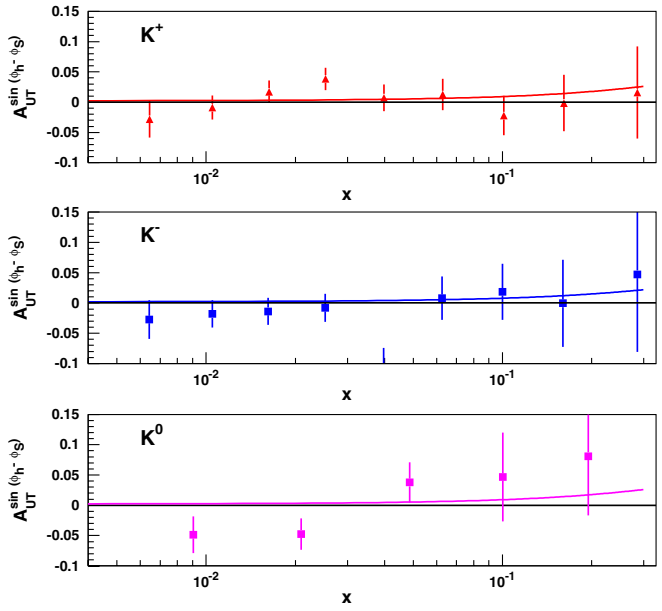

FIG. 8 (color online). Comparisons of our predictions for the Sivers asymmetries in the production of K^+ (top panel), K^- (middle panel), and K^0 (bottom panel) with COMPASS deuteron target data, assuming $\alpha_s = 0.3$ and $\Lambda = 0.65$ GeV for the dipole model parameters.

the case of the HERMES data for kaons, we see qualitative agreement for the K^+ asymmetry shown in the top panel of Fig. 6, though the experimental values are somewhat larger than the predictions, albeit with large errors. This difference could be explained by the fact that we do not include the $\bar{s}$ contribution, which dominates in fragmentation to the K^+. In the case of the K^- asymmetry shown in the lower panel of Fig. 6, the experimental values are similar to the predictions, though again with relatively large errors.

The corresponding comparisons for COMPASS data on pion and kaon production are shown in Figs. 7 and 8, respectively. In this case, again using a dipole form factor and $\alpha_s = 0.3$ and $\Lambda = 0.65$ GeV, we predict small asymmetries for all three charge states for both pions and kaons. These predictions are compatible with the data available from COMPASS for $\pi^\pm$, $K^\pm$, and K^0 production.

We conclude that our model gives qualitatively successful predictions for the Sivers asymmetries if a dipole form factor is assumed.

IV. GAUSSIAN FORM FACTOR

A. Calculations

In order to assist in evaluating the reliability of our results, in this section we make a similar analysis of the predictions for the Sivers asymmetries obtained using a Gaussian form factor at the proton–quark-diquark vertex given by

$$g(k^2) = \sqrt{N_R}(k^2 - m^2)e^{(1/2\Lambda_1^2)(k^2-\Lambda^2)}, \tag{44}$$

where $-k^2 = \frac{\mathbf{k}_\perp^2}{1-x} + \frac{x}{1-x}M_R^2 - xM^2$. In this case, we have the distribution functions

$$f_1^R(x,\mathbf{k}_\perp) = \frac{N_R}{\Lambda_1^2(1-x)} f_0(x)[(xM+m)^2 + \mathbf{k}_\perp^2] \times e^{-(\mathbf{k}_\perp^2/\Lambda_1^2(1-x))}, \tag{45}$$

where

$$f_0(x) = e^{(x(1-x)M^2 - xM_R^2)/(\Lambda_1^2(1-x))}. \tag{46}$$

After integration over $\mathbf{k}_\perp$, we obtain the distribution functions

$$f_1^R(x) = \pi N_R f_0(x)[(xM+m)^2 + \Lambda_1^2(1-x)], \tag{47}$$

where the normalization factors N_R are fixed by

$$\int_0^1 dx f_1^R(x) = 1. \tag{48}$$

We obtain from (27) for the present Gaussian form factor

$$R(x,\mathbf{k}_\perp) \times e^{-(\mathbf{k}_\perp^2/2\Lambda_1^2(1-x))} = \frac{1}{\mathbf{k}_\perp^2}\int_0^{\mathbf{k}_\perp^2} d(\boldsymbol{l}_\perp^2) e^{-(l_\perp^2/2\Lambda_1^2(1-x))} = \frac{1}{\mathbf{k}_\perp^2} 2\Lambda_1^2(1-x) \times (1 - e^{-(\mathbf{k}_\perp^2/2\Lambda_1^2(1-x))}). \tag{49}$$

Finally, we obtain the following Sivers distribution functions for the Gaussian form factor:

$$f_{1T}^{\perp R}(x,\mathbf{k}_\perp) = a_R \frac{e_1 e_2}{4\pi} N_R 2M(xM+m) f_0(x) \times \frac{1}{\mathbf{k}_\perp^2} e^{-(\mathbf{k}_\perp^2/2\Lambda_1^2(1-x))}(1 - e^{-(\mathbf{k}_\perp^2/2\Lambda_1^2(1-x))}), \tag{50}$$

where $a_s = 1$ and $a_a = -\frac{1}{3}$ as in (40). Relevant formulas and details of the derivation and the relation between the light-cone and rest-frame SU(6) descriptions of the nucleon wave function are given in the Appendix.

We present in the top panel of Fig. 9 the dependence of the calculated asymmetry on the upper limit in the $\mathbf{k}_\perp$ integral. As one can see in Figs. 4 and 9, the convergence of the $\mathbf{k}_\perp$ integration is faster with the Gaussian form factor than with the dipole form factor, and in this section we use $|\mathbf{k}_\perp|_{\max} = 1.5$ GeV for the upper limit of the $\mathbf{k}_\perp$ integration. As explained in Sec. III A, because of the strong correlation between the mean values of x and the virtuality of the hard scattering Q^2, and the fact that the simple diquark model used here treats only the valence quarks, the results cannot be considered reliable for low values of x. Hence, our results should be considered as applicable only to $x > 0.1$.

Another issue bearing on the accuracy of our results is that unitarity requires the analyzing power of the Sivers function to be less than unity in modulus for all values of x

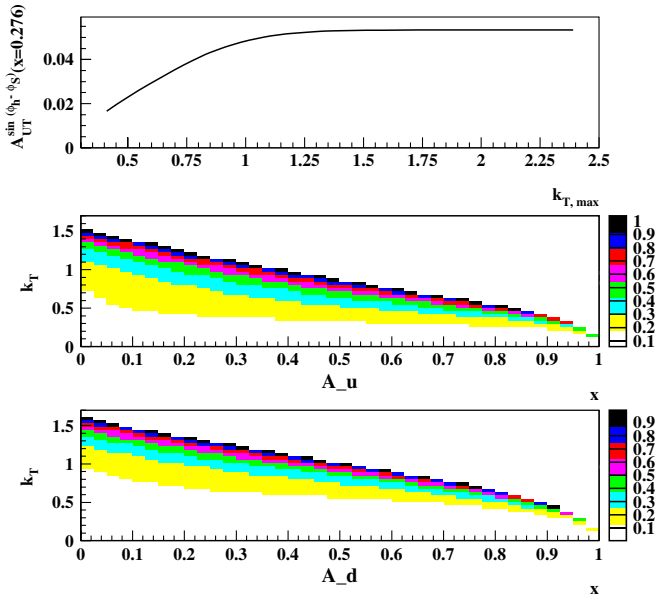

FIG. 9 (color online). In the top panel, we show the Sivers asymmetry for π^+ production off a proton target for HERMES kinematics at $x = 0.276$ as a function of the upper limit of the $|\mathbf{k}_\perp|$ integration. The analyzing power of Sivers function for scattering off a u quark (middle panel) and a d quark (bottom panel) as functions of x and $k_T = |\mathbf{k}_\perp|$. The values exceed the unitarity limit in the white regions at larger x and k_T. All these plots are obtained using Gaussian form factors with parameters $\Lambda_1 = 0.5$ GeV and $\alpha_s = 0.3$.

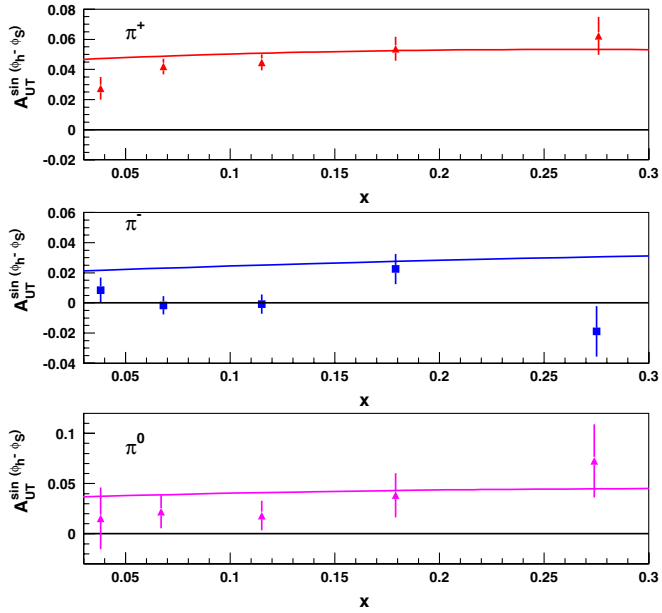

FIG. 10 (color online). Comparisons of our predictions for the Sivers asymmetries in the production of π^+ (top panel), π^- (middle panel) and π^0 (bottom panel) with HERMES data, assuming $\alpha_s = 0.3$ and $\Lambda_1 = 0.5$ GeV for the Gaussian model parameters.

and $\mathbf{k}_\perp$. This is not always the case for the simplified leading-order one-gluon-exchange FSI that we consider, which tends to yield larger values at large x and $\mathbf{k}_\perp$, as seen in the middle panel of Fig. 9 for scattering off a u quark, and in the bottom panel for scattering off a d quark. In order to estimate the error incurred by including unphysical values in the integration over $\mathbf{k}_\perp$, we compared the naive predictions obtained by ignoring the unitarity issue and the modified calculations obtained by truncating the $\mathbf{k}_\perp$ integration at the x-dependent unitarity limit shown in Fig. 9, and found that they differ by far less than the present experimental uncertainties. In reality, the contributions to the integrations of $\Delta\hat{\sigma}(x)$ in (8) and $\hat{\sigma}(x)$ in (9) from the $\mathbf{k}_\perp$ range where unitarity is violated are very small, since due to the Gaussian form factor the integrands of both (8) and (9) decrease very rapidly when $|\mathbf{k}_\perp|$ becomes large. Hence the theoretical error arising from this unitarity issue is estimated to be small.

B. Comparisons with data

We display in Figs. 10 and 11 comparisons of our predictions for the Sivers asymmetries with HERMES data on pion and kaon production, respectively. These predictions are calculated with the Gaussian form factor using $\alpha_s = 0.3$, $\Lambda_1 = 0.5$ GeV. As in the dipole case, we find quantitative success for the π^+ asymmetry and qualitative success for the π^0 asymmetry, while the experimental errors in the π^- asymmetry do not permit a firm conclusion to be drawn. In the case of the $K^\pm$ asymmetries, we again find a qualitative success for the K^+ case, though the measured asymmetry is larger than our prediction. This may again be explained by ignorance of the $\bar{s}$ contribution.

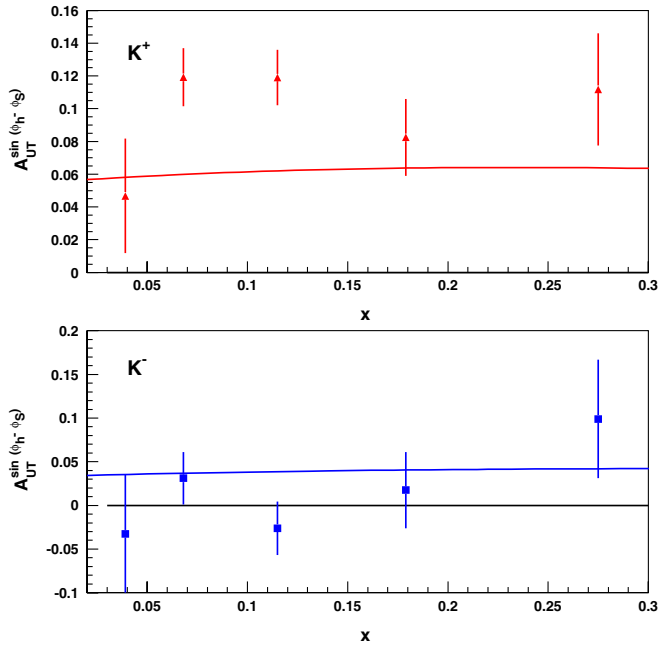

FIG. 11 (color online). Comparisons of our predictions for the Sivers asymmetries in the production of K^+ (top panel) and K^- (bottom panel) with HERMES data, assuming $\alpha_s = 0.3$ and $\Lambda_1 = 0.5$ GeV for the Gaussian model parameters.

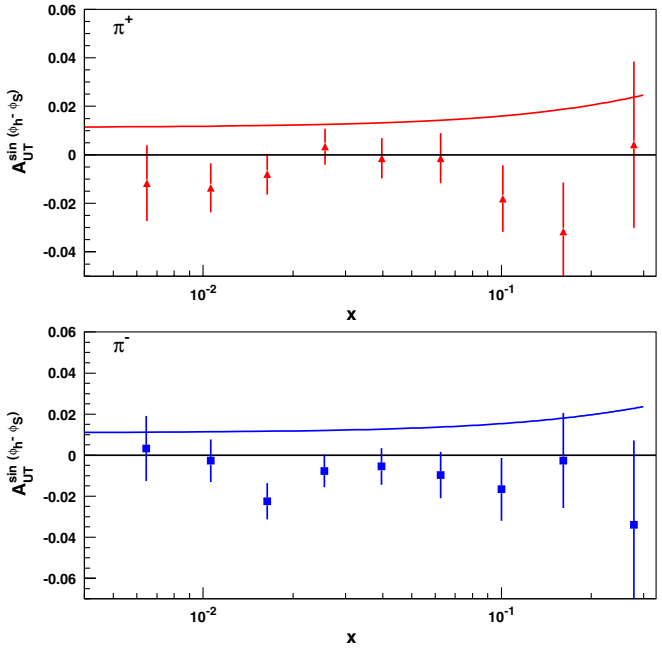

FIG. 12 (color online). Comparisons of our predictions for the Sivers asymmetries in the production of π^+ (top panel), π^- (bottom panel) with COMPASS deuteron data for $\pi^\pm$, assuming $\alpha_s = 0.3$ and $\Lambda_1 = 0.5$ GeV for the Gaussian model parameters.

In the K^- case, the prediction is also qualitatively successful, though no definite conclusion can be drawn.

The corresponding comparisons between our predictions and COMPASS data on pion and kaon production are shown in Figs. 12 and 13, respectively. In the $\pi^\pm$ cases

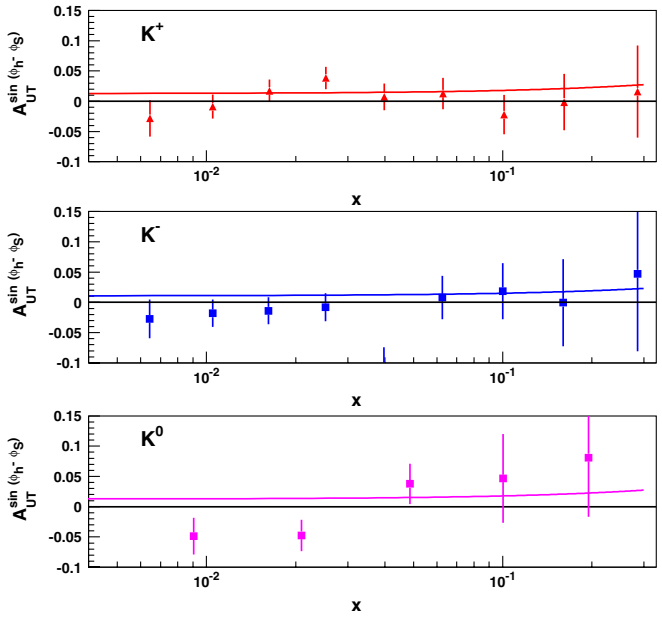

FIG. 13 (color online). Comparisons of our predictions for the Sivers asymmetries in the production of K^+ (top panel), K^- (middle panel), and K^0 (bottom panel) with COMPASS deuteron data, assuming $\alpha_s = 0.3$ and $\Lambda_1 = 0.5$ GeV for the Gaussian model parameters.

we predict smaller Sivers asymmetries than for HERMES, and the data certainly reflect this trend, though the data are quite compatible with zero. In the cases of the kaon asymmetries shown in Fig. 13, the predicted asymmetries are very close to zero, as are the values measured by COMPASS.

We see that our model also gives qualitatively successful predictions for the Sivers asymmetries if a Gaussian form factor is assumed, and that the predictions using this and a dipole form factor are qualitatively similar. This gives some further confidence in the stability of our results and the conclusions we draw.

V. CONCLUSIONS

We have studied the Sivers single-spin asymmetry in SIDIS generated by the mechanism of a one-gluon-exchange final-state interaction. We derived a general formula that can be used to calculate the Sivers distribution function for diquark models having different form factors at the nucleon-quark-diquark vertex. We calculated the Sivers distribution functions in diquark models with both dipole and Gaussian form factors, and compared the corresponding predictions for Sivers single-spin asymmetries in pion and kaon production in SIDIS with the results of HERMES and COMPASS. The predictions made using dipole and Gaussian form factors are quite similar, and are relatively insensitive to the unphysical values of the model calculations at large x and $\mathbf{k}_\perp$.

We find qualitatively successful results for the asymmetries in π^+, π^0, and K^+ production. In the case of K^+ production at HERMES, the measured values are even larger than our predictions, reflecting the possible importance of an $\bar{s}$ contribution. In other cases, particularly at COMPASS energies, many of the experimental measurements are currently compatible with zero, and greater accuracy will be necessary to confront our theoretical predictions. On the theoretical side, it is desirable to improve the accuracy of our predictions, in particular, by going beyond the simple one-gluon-exchange final-state interaction. However, the relative success of this first confrontation between HERMES and COMPASS data and our naive predictions is an encouraging indication that one may be able to understand satisfactorily the Sivers asymmetries in SIDIS, which are rather subtle aspects of hadron dynamics in deep-inelastic scattering.

One *prima facie* conclusion from the successful comparison between our predictions and the HERMES data on π^+, π^0, and K^+ production is that the quark partons in the nucleon must have nonzero orbital angular momentum in the infinite-momentum frame.

ACKNOWLEDGMENTS

We thank Alessandro Bacchetta, Stan Brodsky, Leonard Gamberg, Piet Mulders, Marco Radici, and Misha

Sapozhnikov for helpful discussions. This work was supported in part by the International Cooperation Program of the KICOS (Korea Foundation for International Cooperation of Science & Technology).

APPENDIX A: WAVE FUNCTIONS OF SCALAR AND AXIAL-VECTOR DIQUARK MODELS

The expansion of the proton state in terms of light-cone Fock states is

$$|\psi_p(P^+, \mathbf{P}_\perp)\rangle = \sum_n \prod_{i=1}^n \frac{dx_i d^2\mathbf{k}_{\perp i}}{\sqrt{x_i}16\pi^3} 16\pi^3 \delta\Big(1 - \sum_{i=1}^n x_i\Big) \times \delta^{(2)}\Big(\sum_{i=1}^n \mathbf{k}_{\perp i}\Big)\psi_n(x_i, \mathbf{k}_{\perp i}, \lambda_i) \times |n; x_i P^+, x_i \mathbf{P}_\perp + \mathbf{k}_{\perp i}, \lambda_i\rangle, \tag{A1}$$

where the light-cone momentum fractions $x_i = k_i^+/P^+$ and $\mathbf{k}_{\perp i}$ represent the momenta of the QCD constituents. The physical transverse momenta are $\mathbf{p}_{\perp i} = x_i \mathbf{P}_\perp + \mathbf{k}_{\perp i}$. The λ_i label the light-cone spin projections S^z of the quarks and gluons along the quantization direction z. The n-particle states are normalized as

$$\langle n; p_i'^+, \mathbf{p}'_{\perp i}, \lambda_i' | n; p_i^+, \mathbf{p}_{\perp i}, \lambda_i\rangle = \prod_{i=1}^n 16\pi^3 p_i^+ \delta(p_i'^+ - p_i^+)\delta^{(2)}(\mathbf{p}'_{\perp i} - \mathbf{p}_{\perp i})\delta_{\lambda_i'\lambda_i}. \tag{A2}$$

Here and in the following we do not display the other quantum numbers of the partons, i.e., color and quark flavor.

In order to construct diquark models, we take the following form factors at the proton–quark-diquark vertex, for the scalar (s) and axial-vector (a) diquarks, respectively,

$$\Upsilon_s = g_s(k^2), \qquad \Upsilon_a^\mu = \frac{g_a(k^2)}{\sqrt{3}}\gamma^\mu\gamma_5. \tag{A3}$$

We can then obtain the light-cone wave functions of scalar and axial-vector diquark models from Fig. 14. In this Appendix we consider elementary vertices given by

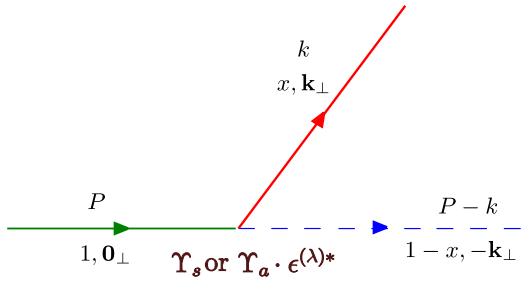

FIG. 14 (color online). Diagram giving the light-cone wave functions of scalar and axial-vector diquark models.

$g_s(k^2) = g_a(k^2) = 1$. In Secs III and IV we introduce dipole and Gaussian form factors, respectively.

1. Scalar diquark model

We also use the term "Yukawa model" for the scalar diquark model described in this subsection. Each Fock-state wave function of the physical proton with total spin projection $J^z = \pm\frac{1}{2}$ is represented by a function $\psi_n^{J^z}(x_i, \mathbf{k}_{\perp i}, \lambda_i)$, where

$$k_i = (k_i^+, \mathbf{k}_{\perp i}, k_i^-) = \Big(x_i P^+, \mathbf{k}_{\perp i}, \frac{\mathbf{k}_{\perp i}^2 + m_i^2}{x_i P^+}\Big) \tag{A4}$$

specifies the momentum of each constituent and λ_i specifies its light-cone helicity in the z direction.

From Fig. 14 with the scalar vertex Υ_s, the $J^z = +\frac{1}{2}$ two-particle Fock state in the scalar diquark model is given by [33,34]

$$|\Psi^\uparrow_{\text{two particle}}(P^+, \mathbf{P}_\perp = \mathbf{0}_\perp)\rangle = \int \frac{dx d^2\mathbf{k}_\perp}{\sqrt{x(1-x)}16\pi^3}\Big[\psi^\uparrow_{+(1/2)}(x, \mathbf{k}_\perp)\Big|+\frac{1}{2}; xP^+, \mathbf{k}_\perp\Big\rangle + \psi^\uparrow_{-(1/2)}(x, \mathbf{k}_\perp)\Big|-\frac{1}{2}; xP^+, \mathbf{k}_\perp\Big\rangle\Big], \tag{A5}$$

where

$$\psi^\uparrow_{+(1/2)}(x, \mathbf{k}_\perp) = \frac{(xM + m)}{x}\varphi, \qquad \psi^\uparrow_{-(1/2)}(x, \mathbf{k}_\perp) = -\frac{(+k^1 + ik^2)}{x}\varphi. \tag{A6}$$

The scalar part of the wave function φ is given by [33,34]

$$\varphi(x, \mathbf{k}_\perp) = \frac{g}{\sqrt{1-x}}\frac{1}{M^2 - \frac{\mathbf{k}_\perp^2 + m^2}{x} - \frac{\mathbf{k}_\perp^2 + \lambda^2}{1-x}} = -g\frac{x\sqrt{1-x}}{\mathbf{k}_\perp^2 + B}, \tag{A7}$$

where M, m, and λ are the masses of proton, quark, and diquark, respectively, and

$$B = x(1-x)\Big(-M^2 + \frac{m^2}{x} + \frac{\lambda^2}{1-x}\Big). \tag{A8}$$

Similarly, the $J^z = -\frac{1}{2}$ two-particle Fock state is given by [33,34]

$$|\Psi^\downarrow_{\text{two particle}}(P^+, \mathbf{P}_\perp = \mathbf{0}_\perp)\rangle = \int \frac{dx d^2\mathbf{k}_\perp}{\sqrt{x(1-x)}16\pi^3}\Big[\psi^\downarrow_{+(1/2)}(x, \mathbf{k}_\perp)\Big|+\frac{1}{2}; xP^+, \mathbf{k}_\perp\Big\rangle + \psi^\downarrow_{-(1/2)}(x, \mathbf{k}_\perp)\Big|-\frac{1}{2}; xP^+, \mathbf{k}_\perp\Big\rangle\Big], \tag{A9}$$

where

$$\psi^{\downarrow}_{+(1/2)}(x,\mathbf{k}_\perp) = -\frac{(-k^1+ik^2)}{x}\varphi,$$
$$\psi^{\downarrow}_{-(1/2)}(x,\mathbf{k}_\perp) = \frac{(xM+m)}{x}\varphi. \tag{A10}$$

The quark-state bases on the right-hand sides of (A5) and (A9) correspond to light-cone spinors (LC). The Bjorken-Drell (BD) spinors $u^{\rm BD}(k)$ and the light-cone spinors $u^{\rm LC}(k)$ are related by

$$u^{\rm BD}_{+(1/2)}(k) = \frac{1}{\sqrt{(k^+ + m)^2 + \vec{k}_\perp^2}}((k^+ + m)u^{\rm LC}_{+(1/2)}(k) - (k^1 + ik^2)u^{\rm LC}_{-(1/2)}(k)),$$
$$u^{\rm BD}_{-(1/2)}(k) = \frac{1}{\sqrt{(k^+ + m)^2 + \vec{k}_\perp^2}}(-(-k^1 + ik^2)u^{\rm LC}_{+(1/2)}(k) + (k^+ + m)u^{\rm LC}_{-(1/2)}(k)). \tag{A11}$$

The Bjorken-Drell spinors $u^{\rm BD}(k)$ satisfy

$$j^+u^{\rm BD}_{+(1/2)}(k) = 0, \qquad j^-u^{\rm BD}_{-(1/2)}(k) = 0,$$
$$j^-u^{\rm BD}_{+(1/2)}(k) = u^{\rm BD}_{-(1/2)}(k), \qquad j^+u^{\rm BD}_{-(1/2)}(k) = u^{\rm BD}_{+(1/2)}(k), \tag{A12}$$

where $j^\pm = j^1 \pm ij^2$ and

$$j^i = s^i + l^i, \qquad s^i = \Sigma^i = \begin{pmatrix}\sigma^i & 0\\ 0 & \sigma^i\end{pmatrix},$$
$$l^i = -i\epsilon^{ijk}k^j\frac{\partial}{\partial k^k}, \qquad \epsilon^{123} = 1. \tag{A13}$$

Since $k^+ = xM$ in the proton rest frame, from (A11) the Fock states given in (A5) and (A9) with the light-cone wave functions (A6) and (A10) correspond to $|+\frac{1}{2}; xP^+, \mathbf{k}_\perp\rangle^{\rm BD}$ and $|-\frac{1}{2}; xP^+, \mathbf{k}_\perp\rangle^{\rm BD}$, respectively, in the proton rest frame.

2. Axial-vector diquark model

For the polarization vectors of the axial-vector diquark appearing at the vertex of Fig. 14, we use the following set of three polarization vectors:

$$\epsilon^{(+1)\mu} = (\epsilon^{(+1)0}, \epsilon^{(+1)1}, \epsilon^{(+1)2}, \epsilon^{(+1)3}) = \frac{1}{\sqrt{2}}(0,-1,-i,0),$$
$$\epsilon^{(-1)\mu} = \frac{1}{\sqrt{2}}(0,+1,-i,0),$$
$$\epsilon^{(0)\mu} = \left(\frac{P^3}{M},0,0,\frac{P^0}{M}\right). \tag{A14}$$

These polarization vectors are those used in Ref. [19] which satisfy $\sum_\lambda \epsilon^{(\lambda)*}_\mu \epsilon^{(\lambda)}_\nu = -g_{\mu\nu} + P_\mu P_\nu/M^2$. In the proton rest frame, $\epsilon^{(0)\mu}$ is the spin vector oriented in the z direction and $\epsilon^{(\pm1)\mu}$ are those circularly polarized in the x-y plane.

From Fig. 14 with the scalar vertex $\Upsilon_a \cdot \epsilon^{(\lambda)*}$, the two-particle Fock state for the proton with $J^z = +\frac{1}{2}$ has six possible spin combinations for the quark and axial-vector diquark:

$$|\Psi^{\uparrow}_{\text{two particle}}(P^+, \mathbf{P}_\perp = \mathbf{0}_\perp)\rangle = \int \frac{dxd^2\mathbf{k}_\perp}{\sqrt{x(1-x)}16\pi^3}\Big[\psi^{\uparrow}_{+(1/2)+1}(x,\mathbf{k}_\perp)\Big|+\frac{1}{2}+1; xP^+, \mathbf{k}_\perp\Big\rangle + \psi^{\uparrow}_{-(1/2)+1}(x,\mathbf{k}_\perp)\Big|-\frac{1}{2}+1; xP^+, \mathbf{k}_\perp\Big\rangle + \psi^{\uparrow}_{+(1/2)0}(x,\mathbf{k}_\perp)\Big|+\frac{1}{2}0; xP^+, \mathbf{k}_\perp\Big\rangle + \psi^{\uparrow}_{-(1/2)0}(x,\mathbf{k}_\perp)\Big|-\frac{1}{2}0; xP^+, \mathbf{k}_\perp\Big\rangle + \psi^{\uparrow}_{+(1/2)-1}(x,\mathbf{k}_\perp)\Big|+\frac{1}{2}-1; xP^+, \mathbf{k}_\perp\Big\rangle + \psi^{\uparrow}_{-(1/2)-1}(x,\mathbf{k}_\perp)\Big|-\frac{1}{2}-1; xP^+, \mathbf{k}_\perp\Big\rangle\Big], \tag{A15}$$

where the two-particle states $|s^z_{\rm f}, s^z_{\rm b}; x, \mathbf{k}_\perp\rangle$ are normalized as in (A2). Here $s^z_{\rm f}$ and $s^z_{\rm b}$ denote the z component of the spins of the constituent fermion and boson, respectively, and the variables x and $\mathbf{k}_\perp$ refer to the momentum of the fermion. The wave functions are given by

$$\psi^{\uparrow}_{+(1/2)+1}(x,\mathbf{k}_\perp) = -\sqrt{\frac{2}{3}}\frac{(-k^1+ik^2)}{x}\varphi, \qquad \psi^{\uparrow}_{-(1/2)+1}(x,\mathbf{k}_\perp) = +\sqrt{\frac{2}{3}}\frac{(xM+m)}{x}\varphi,$$
$$\psi^{\uparrow}_{+(1/2)0}(x,\mathbf{k}_\perp) = -\sqrt{\frac{1}{3}}\frac{(xM+m)}{x}\varphi, \qquad \psi^{\uparrow}_{-(1/2)0}(x,\mathbf{k}_\perp) = +\sqrt{\frac{1}{3}}\frac{(+k^1+ik^2)}{x}\varphi,$$
$$\psi^{\uparrow}_{+(1/2)-1}(x,\mathbf{k}_\perp) = 0, \qquad \psi^{\uparrow}_{-(1/2)-1}(x,\mathbf{k}_\perp) = 0, \tag{A16}$$

where

$$\varphi(x, \mathbf{k}_\perp) = \frac{e}{\sqrt{1-x}} \frac{1}{M^2 - \frac{\mathbf{k}_\perp^2 + m^2}{x} - \frac{\mathbf{k}_\perp^2 + \lambda^2}{1-x}}. \tag{A17}$$

Similarly, the wave functions for a proton with negative helicity are given by

$$\begin{aligned}
&\psi^\downarrow_{+(1/2)+1}(x, \mathbf{k}_\perp) = 0, \qquad \psi^\downarrow_{-(1/2)+1}(x, \mathbf{k}_\perp) = 0, \qquad \psi^\downarrow_{+(1/2)0}(x, \mathbf{k}_\perp) = -\sqrt{\frac{1}{3}} \frac{(-k^1 + ik^2)}{x} \varphi, \\
&\psi^\downarrow_{-(1/2)0}(x, \mathbf{k}_\perp) = +\sqrt{\frac{1}{3}} \frac{(xM + m)}{x} \varphi, \qquad \psi^\downarrow_{+(1/2)-1}(x, \mathbf{k}_\perp) = -\sqrt{\frac{2}{3}} \frac{(xM + m)}{x} \varphi, \\
&\psi^\downarrow_{-(1/2)-1}(x, \mathbf{k}_\perp) = +\sqrt{\frac{2}{3}} \frac{(+k^1 + ik^2)}{x} \varphi.
\end{aligned} \tag{A18}$$

The coefficients of φ in (A16) and (A18) are the matrix elements of $\frac{\bar{u}(k^+, k^-, \mathbf{k}_\perp)}{\sqrt{k^+}} \Upsilon_a \cdot \epsilon^{(\lambda)*} \frac{u(P^+, P^-, \mathbf{P}_\perp)}{\sqrt{P^+}}$, which are the numerators of the wave functions corresponding to each constituent-spin s^z configuration.

Because of the transformation properties (A12) of the Bjorken-Drell spinors $u^{\mathrm{BD}}(k)$, when we construct the proton spin states $|P; \lambda = \pm\frac{1}{2}\rangle$ by using the Clebsch-Gordan coefficients with $u^{\mathrm{BD}}(k)$ for spin-half components, they satisfy

$$\begin{aligned}
&J^+ \left| P; \lambda = +\frac{1}{2} \right\rangle = 0, \\
&J^- \left| P; \lambda = -\frac{1}{2} \right\rangle = 0 \\
&J^- \left| P; \lambda = +\frac{1}{2} \right\rangle = \left| P; \lambda = -\frac{1}{2} \right\rangle, \\
&J^+ \left| P; \lambda = -\frac{1}{2} \right\rangle = \left| P; \lambda = +\frac{1}{2} \right\rangle,
\end{aligned} \tag{A19}$$

where J^i is the angular momentum operator for the proton given by $J^i = \sum_a j^i_a = \sum_a (s^i_a + l^i_a)$, which is the sum over the constituents a, and $J^\pm = J^1 \pm iJ^2$.

Since $k^+ = xM$ in the proton rest frame, from (A11) the Fock states with the light-cone wave functions given in (A16) and (A18) correspond to the following states in the proton rest-frame, respectively:

$$\left(\sqrt{\frac{2}{3}} \left| -\frac{1}{2} + 1; xP^+, \mathbf{k}_\perp \right\rangle^{\mathrm{BD}} - \sqrt{\frac{1}{3}} \left| +\frac{1}{2} 0; xP^+, \mathbf{k}_\perp \right\rangle^{\mathrm{BD}}\right),$$

$$\left(-\sqrt{\frac{2}{3}} \left| +\frac{1}{2} - 1; xP^+, \mathbf{k}_\perp \right\rangle^{\mathrm{BD}} + \sqrt{\frac{1}{3}} \left| -\frac{1}{2} 0; xP^+, \mathbf{k}_\perp \right\rangle^{\mathrm{BD}}\right).$$

The above states are angular momentum eigenstates $|P; \lambda = +\frac{1}{2}\rangle$ and $|P; \lambda = -\frac{1}{2}\rangle$, respectively, which satisfy (A19). In the proton rest frame, the states described by (A16) and (A18) are identical to the axial-vector diquark states appearing in the SU(6) wave functions (28) and (29). Therefore, in the proton rest frame the wave functions of the axial-vector diquark states derived here through the vertex given in Fig. 14 with the polarization vectors given in (A14) coincide with those in the SU(6) wave function for the proton.

[1] D. W. Sivers, Phys. Rev. D **41**, 83 (1990); **43**, 261 (1991).
[2] J. C. Collins, Nucl. Phys. **B396**, 161 (1993).
[3] M. Anselmino, M. Boglione, and F. Murgia, Phys. Lett. B **362**, 164 (1995).
[4] D. Boer and P. J. Mulders, Phys. Rev. D **57**, 5780 (1998).
[5] D. L. Adams *et al.* (FNAL-E704 Collaboration), Phys. Lett. B **264**, 462 (1991).
[6] S. J. Brodsky, D. S. Hwang, and I. Schmidt, Phys. Lett. B **530**, 99 (2002).
[7] A. Airapetian *et al.* (HERMES Collaboration), Phys. Rev. Lett. **94**, 012002 (2005).
[8] M. Diefenthaler (HERMES Collaboration), arXiv:0706.2242; *Proceedings of 15th International Workshop on Deep-Inelastic Scattering and Related Subjects (DIS2007)* (Munich, Germany, 2007), pp. 579–582.
[9] M. Alekseev *et al.* (COMPASS Collaboration), Phys. Lett. B **673**, 127 (2009).
[10] W. Vogelsang and F. Yuan, Phys. Rev. D **72**, 054028 (2005).
[11] J. C. Collins, A. V. Efremov, K. Goeke, S. Menzel, A. Metz, and P. Schweitzer, Phys. Rev. D **73**, 014021 (2006).
[12] S. Arnold, A. V. Efremov, K. Goeke, M. Schlegel, and P. Schweitzer, arXiv:0805.2137.
[13] M. Anselmino *et al.*, Eur. Phys. J. A **39**, 89 (2009).
[14] D. Boer and W. Vogelsang, Phys. Rev. D **69**, 094025 (2004).
[15] A. Bacchetta, C. J. Bomhof, P. J. Mulders, and F. Pijlman,

Phys. Rev. D **72**, 034030 (2005).
[16] B. I. Abelev *et al.* (STAR Collaboration), Phys. Rev. Lett. **99**, 142003 (2007).
[17] P. J. Mulders and R. D. Tangerman, Nucl. Phys. **B461**, 197 (1996); **B484**, 538(E) (1997).
[18] S. J. Brodksy, D. S. Hwang, and I. Schmidt, Phys. Lett. B **553**, 223 (2003).
[19] R. Jakob, P. J. Mulders, and J. Rodrigues, Nucl. Phys. **A626**, 937 (1997).
[20] A. Bacchetta, A. Schäfer, and J. J. Yang, Phys. Lett. B **578**, 109 (2004).
[21] A. Bacchetta, F. Conti, and M. Radici, Phys. Rev. D **78**, 074010 (2008).
[22] L. P. Gamberg, G. R. Goldstein, and M. Schlegel, Phys. Rev. D **77**, 094016 (2008).
[23] L. P. Gamberg, G. R. Goldstein, and K. A. Oganessyan, Phys. Rev. D **67**, 071504 (2003).
[24] L. P. Gamberg, G. R. Goldstein, and K. A. Oganessyan, Phys. Rev. D **68**, 051501 (2003).
[25] J. C. Collins, Phys. Lett. B **536**, 43 (2002).
[26] X. Ji and F. Yuan, Phys. Lett. B **543**, 66 (2002).
[27] A. Belitsky, X. Ji, and F. Yuan, Nucl. Phys. **B656**, 165 (2003).
[28] D. Boer, P. J. Mulders, and F. Pijlman, Nucl. Phys. **B667**, 201 (2003).
[29] D. Boer, S. J. Brodsky, and D. S. Hwang, Phys. Rev. D **67**, 054003 (2003).
[30] W. Melnitchouk, A. W. Schreiber, and A. W. Thomas, Phys. Rev. D **49**, 1183 (1994).
[31] M. Anselmino, M. Boglione, U. D'Alesio, A. Kotzinian, F. Murgia, and A. Prokudin, Phys. Rev. D **71**, 074006 (2005).
[32] D. de Florian, R. Sassot, and M. Stratmann, Phys. Rev. D **75**, 114010 (2007).
[33] S. J. Brodsky and S. D. Drell, Phys. Rev. D **22**, 2236 (1980).
[34] S. J. Brodsky, D. S. Hwang, B.-Q. Ma, and I. Schmidt, Nucl. Phys. **B593**, 311 (2001).